RESEARCH ARTICLE

Nanoparticles

Biotechnology Journal

www.biotechnology-journal.com

Cell-Nanoparticle Interactions at (Sub)-Nanometer Resolution Analyzed by Electron Microscopy and Correlative Coherent Anti-Stokes Raman Scattering

Jukka Saarinen, Friederike Gütter, Mervi Lindman, Mikael Agopov, Sara J. Fraser-Miller, Regina Scherließ, Eija Jokitalo, Hélder A. Santos, Leena Peltonen, Antti Isomäki, and Clare J. Strachan**

A wide variety of nanoparticles are playing an increasingly important role in drug delivery. Label-free imaging techniques are especially desirable to follow the cellular uptake and intracellular fate of nanoparticles. The combined correlative use of different techniques, each with unique advantages, facilitates more detailed investigation about such interactions. The synergistic use of correlative coherent anti-Stokes Raman scattering and electron microscopy (C-CARS-EM) imaging offers label-free, chemically-specific, and (sub)-nanometer spatial resolution for studying nanoparticle uptake into cells as demonstrated in the current study. Coherent anti-Stokes Raman scattering (CARS) microscopy offers chemically-specific (sub)micron spatial resolution imaging without fluorescent labels while transmission electron microscopy (TEM) offers (sub)-nanometer scale spatial resolution and thus visualization of precise nanoparticle localization at the sub-cellular level. This proof-of-concept imaging platform with unlabeled drug nanocrystals and macrophage cells revealed good colocalization between the CARS signal and electron dense nanocrystals in TEM images. The correlative TEM images revealed subcellular localization of nanocrystals inside membrane bound vesicles, showing multivesicular body (MVB)-like morphology typical for late endosomes (LEs), endolysosomes, and phagolysosomes. C-CARS-EM imaging has much potential to study the interactions between a wide range of nanoparticles and cells with high precision and confidence.

1. Introduction

Much attention is being devoted to the use of nanoparticles to overcome several issues related to drug treatment and facilitate the development of efficient and safe medicines. They can be used, for example, to improve the bioavailability of poorly water-soluble drugs or for targeted drug delivery, especially in cancer treatment.[1] Suitable imaging techniques are required to follow the precise fate of these nanoparticles in biological matrices, such as cells and tissues. This is especially important when nanomedicines are used to carry the active pharmaceutical ingredient (API) into the cell, when the biological target is located intracellularly.[2] Cellular internalization of nanoparticles can occur via different endocytosis mechanisms depending on the cell type and physicochemical properties of the nanoparticles, e.g., particle shape and surface charge.[2] The most common technique used to image cells, tissues, and cellular uptake of nanoparticles is fluorescence microscopy.[3] Even though fluorescence

Dr. J. Saarinen, Dr. M. Agopov, Dr. S. J. Fraser-Miller, Prof. H. A. Santos, Dr. L. Peltonen, Prof. C. J. Strachan
Drug Research Program, Division of Pharmaceutical Chemistry
University of Helsinki
Viikinkaari 5 E (PO Box 56), 00014 Helsinki, Finland
E-mail: jukka.saarinen@helsinki.fi; clare.strachan@helsinki.fi

Prof. H. A. Santos
Helsinki Institute of Life Science (HiLIFE)
University of Helsinki
Viikinkaari 5 E (PO Box 56), 00014 Helsinki, Finland

DOI: 10.1002/biot.201800413

Dr. F. Gütter, Prof. R. Scherließ
Pharmaceutical Institute
Department of Pharmaceutics and Biopharmaceutics
Faculty of Mathematics and Natural Sciences
Kiel University
Grasweg 9a, 24118 Kiel, Germany

M. Lindman, Dr. E. Jokitalo
Institute of Biotechnology, Electron Microscopy Unit
University of Helsinki
Viikinkaari 9 (PO Box 56), 00014 Helsinki, Finland

Dr. S. J. Fraser-Miller
Dodd-Walls Centre, Department of Chemistry
University of Otago
PO Box 56, 9056 Dunedin, New Zealand

Dr. A. Isomäki
Biomedicum Imaging Unit
Faculty of Medicine
University of Helsinki
Haartmaninkatu 8 (PO Box 63), 00014 Helsinki, Finland

microscopy allows efficient visualization of nanoparticles and diverse cell organelles, labeling is required in the absence of autofluorescence. There are drawbacks to labeling nanoparticles. Such labels can affect drug function and delivery. Also, fluorescent probes can cause errors in interpretation if they detach from the nanoparticles.[4] Furthermore, photobleaching can render the drug invisible for detection and fluorescent markers can be phototoxic to cells.[3] Fluorescence labeling can also be rather difficult or impossible. One such example is with top-down prepared non-fluorescent drug nanocrystals, and at the same time these represent one of the most widely used classes of nanoparticles in the pharmaceutical industry.

To avoid these drawbacks, label-free analytical techniques are desirable. Among these, vibrational spectroscopic methods are especially promising for directly visualizing biological specimens and nanoparticulate drug delivery systems. These techniques include those based on infrared[5] and Raman spectroscopies.[6] Spontaneous Raman imaging has been used for example to visualize deuterated liposomes,[7] polystyrene nanoparticles,[8] and β-carotene loaded poly(D,L-lactide-co-glycolide) (PLGA) nanoparticles[9] in cells. However, there are several challenges to using spontaneous Raman scattering. The spontaneous Raman scattering cross section is small (the Raman scattering process is relatively rare), making image acquisition slow.[10] This limits its application in the analysis of biological specimens. Also drug concentrations inside the cells tend to be low, which further exacerbates issues with sensitivity and acquisition time.

To overcome these challenges, and slow image acquisition in particular, coherent Raman imaging techniques can be employed. Coherent anti-Stokes Raman scattering (CARS) microscopy is one such technique.[10] CARS microscopy exploits a four-wave mixing process, where three ultra-fast laser pulses are tightly focused through a high numerical aperture (NA) objective and coherently drive molecular vibrations in the small focal volume. At this point, the laser beams are spatially and temporally overlapped, creating a fourth photon, which is then detected. This process makes the technique inherently confocal and allows rapid, label-free, non-destructive, three-dimensional imaging, with the signal originating from molecular vibrational resonances.[11] In addition, one-photon fluorescence interference can be avoided, since the detected anti-Stokes signal is blue-shifted from the excitation frequencies.[11] This technique has become popular in biomedical applications involving cell and tissue imaging; most often via detection of the CH_2 stretching vibrations in cellular lipid structures.[12] The number of publications where this technique has been used to image nanoparticle drug delivery is limited but increasing,[13,14] highlighting the potential value of CARS in the field of drug development and delivery.

Electron microscopy (EM) is a label-free method that has been widely used to image cells containing nanoparticles. In this technique, an electron beam is used as a source of illumination and scattered electrons create image contrast. EM has the obvious benefit of (sub)-nanometer scale spatial resolution that allows visualization of the whole cellular content including different organelles. It therefore follows that visualization of the precise location of individual nanoparticles inside cell organelles is possible.[15] However, this technique lacks chemical-specificity which can prevent, for example, correct identification of intracellular nanoparticles.

Correlative light–electron microscopy (CLEM) is a technique that conventionally combines fluorescence microscopy and electron microscopy to image exactly the same region of interest, such as part of a cell or certain cell organelle, consecutively with both techniques.[16] While other imaging techniques capable of low nanometer resolution also exist, such as super-resolution microscopy[17] and tip-enhanced Raman imaging,[18] EM remains the only imaging technique that can be used to visualize whole cells in great detail, including different organelles and associated membranes in a single image. Despite the potential value of CLEM in the studies of cellular drug delivery of nanoparticles, the number of publications in the area is minimal. Recently, stimulated emission depletion (STED) microscopy was combined with EM to image the cellular uptake of fluorescent nanodiamonds.[19]

In the current study, CARS was synergistically combined with TEM in a correlative manner (C-CARS-EM) to visualize biological specimens and the cellular uptake of non-fluorescent drug nanocrystals. Nanocrystals represent a comparatively simple but difficult/impossible to label nanoparticle model for this proof-of-concept study, with the added benefit that they are widely used in the pharmaceutical industry. CARS microscopy provides label-free chemically-specific imaging on the (sub)-micronscale based on molecular vibrations, while TEM, with its (sub)-nanoscale spatial resolution, provides further information about the subcellular localization and interaction of these drug nanocrystals. The correlative imaging setup presented, with existing methods, allows insights into nanoparticle uptake as well as image interpretation confidence that would not be possible with either technique alone.

2. Experimental Section

2.1. Cell Culturing

RAW 264.7 (ATCC TIB-71) macrophage cells were obtained from ATCC, USA. Cells were cultured at 37 °C and in 5% CO_2. Cells were grown in a 75 cm^2 cell culturing flask (Corning Inc., USA) and passaged every 2 to 3 days. Cell culture medium solution, Dulbecco's Modified Eagle's Medium (DMEM), fetal bovine serum (10% in total) (FBS), L-glutamine, non-essential amino acids (NEAA), penicillin (100 IU mL^{-1}), and streptomycin (100 mg mL^{-1}) were purchased from GE Healthcare, UK. Sodium pyruvate (1% in total) was purchased from Thermo Fisher Scientific, USA. Cells were passaged using cell scrapers (Corning Inc., product no# 3010) with cells being washed twice with DMEM and 10 mL of DMEM being added to the flask prior to scraping to detach the cells. Approximately 1 mL of cell suspension was added to a new culturing flask with 13 mL of DMEM in total. For the uptake studies, cells with passage numbers below 10 were used.

2.2. Preparation of Nanosuspensions

GLI-NC suspensions were prepared via media milling using a Dispermat SL-C 5 bead mill (VMA Getzmann GmbH,

Germany). The suspension medium was double-distilled water (FinnAqua 75, San Asalo-Sohlberg Corp., Helsinki, Finland) and the suspension was stabilized with hydroxypropylmethyl cellulose (HPMC) (METHOCEL E5 Premium LV, Dow Chemical Company, Stade, Germany) (10% w/w relative to the drug). The milling was performed for 320 min in circulation mode with a pump speed of 70 mL min^{-1}, rotor speed of 4000 rpm and silica beads with a size of 1–1.2 mm. The batch size was 100 g with 10 g of glibenclamide (Alpha Aesar, Karlsruhe, Germany).

2.3. CARS Microscopy

A Leica TCS SP8 CARS microscope (Leica, Germany) was used for bright field (BF), CARS and two-photon fluorescence (TPEF) imaging. The microscope consists of an inverted microscope with a laser-scanning confocal scan-head and photomultiplier tube (PMT) and GaAsP hybrid (HyD) photodetectors. The CARS excitation source (Stokes) was a Nd:YVO_4 laser with a wavelength of 1064.5 nm. The pump and probe beams were generated using an optical parametric oscillator (OPO). The bandwidth of the Stokes beam was about 2–3 cm^{-1} and the repetition rate was 80 MHz. The pulse duration was 7 ps for the Stokes and 5–6 ps for the pump and probe beams. A water-immersion 25 × objective with a NA of 0.95 (Leica HCX IR APO L 25 × /0.95 W) was used. Average powers at the focus were approximately 30 mW for Stokes beam and 43 mW for pump/probe beam. The CARS spectra of glibenclamide (GLI), HPMC and glibenclamide nanocrystal (GLI-NC) suspensions were measured by placing a small amount of powder or suspension on a coverslip and systematically changing the wavelength of the pump laser from 797 to 821 nm with 41 steps.

A HeNe laser with a wavelength of 633 nm and a power below 0.1 mW was used for BF imaging. The transmitted light was detected with a PMT detector. The Stokes beam (1064.5 nm, power 50 mW) was used to excite the CellMask Orange (Life Technologies Corp., Carlsbad, CA, USA), for visualizing the cells. The TPEF signal was detected with a HyD detector (detection range 450–550 nm). Images were acquired with Leica Application Suite Advanced Fluorescence (LASAF) software. Spectral processing was performed using OriginPro 8.6 (OriginLab, Northampton, Massachusetts, USA).

2.4. Scanning Electron Microscopy

A FEI Quanta 250 Field Emission Gun Scanning Electron Microscope (FEI, USA) was used to image unmilled GLI powder and dried GLI-NC suspension. The samples were mounted on aluminium stubs covered with carbon tape and then coated with a thin layer of platinum. Micrographs were taken under low (unmilled GLI) or high (GLI-NCs) vacuum, with a 10 kV beam and a spot size of 4 (arbitrary units).

2.5. C-CARS-EM Workflow and Image Acquisition

Cells were seeded on gridded glass-bottomed Petri dishes (MatTek, No. 1.5, 35 mm, 13 mm glass diameter). RAW 264.7 macrophage cells (approximately 100 000 cells per well) were allowed to attach to the bottom of the dish overnight. GLI-NC suspension diluted to a concentration of 250 μg mL^{-1} in DMEM (2 mL) was added and cells were incubated at 37 °C and 5% CO_2 with suspension for 6 h. Excess particles were removed and the cells were washed twice with DMEM. Cell membranes were stained with CellMask Orange plasma membrane stain (5 μg mL^{-1} in DMEM) by incubating the cells in 37 °C and 5% CO_2 with 1 mL of stain for 5 min. The stain solution was then removed and cells were fixed with glutaraldehyde (2%) (Sigma–Aldrich, Germany) in sodium cacodylate buffer (100 mM) (Electron Microscopy Sciences, EMS, USA) for 30 min at room temperature. Sodium cacodylate was replaced with Hank's balanced salt solution (HBSS, Life Technologies, USA) with 2-[4-(2-hydroxyethyl)piperazin-1-yl]ethanesulfonic acid (HEPES, Sigma-Aldrich, Germany) (10 mM) pH 7.4 buffer solution and cells were imaged first with the CARS microscope. BF images with the grid markings were recorded to later locate the same cells for the preparation of TEM sections and subsequent TEM imaging. CARS/TPEF imaging of the cells was performed with z-stack images being recorded (step size 0.5 μm, CARS shift 3075 cm^{-1}). In addition, CARS spectra from inside the cell were recorded by systemically tuning the pump laser 41 times to obtain spectra between 2785 and 3150 cm^{-1}. Cells were then post-fixed with reduced osmiumtetroxide (1%) (Electron Microscopy Sciences, USA) in Na-cacodylate buffer (100 mM), pH 7.4 for 1 h at room temperature, dehydrated with graded series of ethanol (70, 96, and 100%), incubated with transitional solvent acetone and flat-embedded in Epon (TAAB Laboratories Equipment Ltd, UK).[20] About 120 nm thick parallel sections were then cut from the block face using a Leica UCT ultramicrotome, with the area selected based on the bright field images showing the grid markings. Sections were post-stained with uranyl acetate and lead citrate and imaged with a Jeol JEM-1400 TEM (Jeol Ltd., Tokyo, Japan) equipped with a Gatan Orius SC1000B bottom mounted CCD-camera using a 80 kV beam. Entire cells were sectioned and imaged, allowing for comparison of the entire cells imaged with both imaging techniques. For TEM imaging of GLI-NCs without cells, the suspension was diluted with Milli-Q water and a small droplet was placed on a copper grid and allowed to dry prior to imaging.

The Leica Application Suite Advanced Fluorescence (LASAF) was used for image acquisition of CARS/TPEF and BF images and adjusting the contrast for the images. The spectral data was processed with OriginPro 8.6 (OriginLab). Contrast for TEM images was adjusted with Fiji Image J (open-source distribution) and Microscopy Image Browser (MIB, version 2.01 with MATLAB R2017b, MathWork, MA, USA)[21] and overlaying of CARS/TPEF and TEM images was achieved by using GNU Image Manipulation Program v2 (open-source distribution). For the overlaid CARS/TPEF and TEM images, a CARS/TPEF image of size 768 × 768 pixels, obtained with a digital magnification of 4.5× (pixel size 135 nm), was used as a template so that low magnification (500×) TEM images could be compared and overlaid (low magnification of TEM and relatively high magnification of CARS). Furthermore, smaller regions (250 × 250 pixels) within the images were cropped and the CARS/TPEF images within this region were positioned as the bottom layer with the opacity adjusted. Distinguishable regions of the cells (e.g. edges of the cell) were used as a benchmark for

overlaying. The TEM images required some stretching, since sample preparation causes some shrinkage to the cells. For the Video S1, Supporting Information and minimum projection image of overlaid TEM sections (Figure S6, Supporting Information), all the TEM slices were aligned using Amira (version 6.3, Thermo Fisher Scientific, FEI, Oregon, USA). The frame numbers were added to the aligned images using GNU Image Manipulation Program v2 and the final video was rendered in MIB.

3. Results and Discussion

3.1. Preparation and Characterization of Nanocrystals

Unlabeled GLI-NCs were used as the model nanoparticles. GLI-NC suspensions were prepared using media milling. Scanning electron microscopy (SEM) revealed that coarse GLI crystals had prismatic morphology and individual crystals sized up to 100 µm (**Figure 1**A). Particle size reduction to the nanoscale upon milling was confirmed by dynamic light scattering (z-average 252 nm) (Figure S1, Supporting Information) and electron microscopy (Figure 1B and C). In the TEM images, drug nanocrystals appeared as dark electron-dense regions (Figure 1C). X-ray diffraction was used to confirm that the nanoparticles remained crystalline after milling (Figure S2, Supporting Information).

Raman and CARS spectra of coarse GLI crystals and GLI-NCs revealed peaks due to CH_2 and CH_3 stretching at approximately 2840 cm^{-1} (symmetric CH_2 stretching),[22] 2890 cm^{-1} (symmetric and asymmetric CH_2 stretching),[23] and 2935 cm^{-1} (symmetric CH_3 stretching)[24] (Figure 1H and S3, Supporting Information). A peak at 3075 cm^{-1} is due to CH stretching in the benzene ring.[25] This peak was chosen for chemically-specific imaging of GLI crystals with narrowband CARS microscopy (Figure 1E–G), since it is distinct from the CH stretching signals of endogenous cellular lipids observed at 2856 and 2931 cm^{-1} [26] and the stabilizer, hydroxypropylmethyl cellulose (HPMC) (Figure 1H).

3.2. Cellular Uptake Studies

RAW 264.7 macrophage cells were used in drug nanocrystal cellular uptake analysis. These cells were selected because macrophage cells efficiently internalize particles with varied sizes, providing a suitable model for this proof-of-concept study. Control cells (Figure S4, Supporting Information) were used to confirm that cells not incubated with GLI-NCs did not show significant CARS signal at 3075 cm^{-1}.

Cells were incubated with GLI-NCs in cell culturing medium for 6 h and cell membranes were stained with CellMask Orange and fixed with glutaraldehyde. First, cells were imaged with BF microscopy, which was also used to visualize the grid markings on the Petri dishes so that the same cells could later be located and imaged with TEM. Epi-CARS imaging was subsequently performed to probe the GLI-NCs, while cell membranes were visualized with two-photon excited fluorescence (TPEF) using a 1064.5 nm laser (Stokes beam). Epi-CARS detection has the benefit that it efficiently rejects solvent signal and allows highly sensitive imaging of small features such as intracellular features or drug nanocrystals in this case.[27] Therefore, epi-CARS imaging at 3075 cm^{-1} was used to chemically-specifically image GLI-NCs. In addition to CARS imaging, the same cells were imaged with TEM to combine its (sub)-nanometer scale spatial resolution with CARS microscopy as depicted in the workflow chart in **Figure 2**A. Thus, a C-CARS-EM imaging platform, suitable for imaging of drug nanoparticle uptake in more detail with both chemical-specificity and (sub)-nanometer scale spatial resolution, was developed (Figure 2B).

Based on the BF images (**Figure 3**A), GLI-NCs accumulated in the vicinity of the cells after incubation. Confocal TPEF/CARS images could, moreover, be used to confirm that GLI-NCs were inside the cells (Figure 3B). In the C-CARS-EM analysis, correlative CARS/TPEF and low magnification (500×) TEM images provided first a general view of a larger region of the cell (Figure 3C–E). The information obtained from these overview images from the corresponding three cells revealed the regions of interest in which the localization of dark electron-dense crystals in cells was in good correlation with the crystals imaged with CARS (Figure 3C–E). Furthermore, in addition to single peak epi-CARS imaging (at 3075 cm^{-1}), the CARS spectral information could be used to confirm the chemical composition of the overlaid spots and serve as a guide for the higher magnification TEM images (**Figure 4**). It was confirmed that the epi-CARS signal was due to the GLI based on the comparison of the spectra measured inside the cell to the reference spectrum of GLI-NCs, which exhibited similar features, most importantly the peak at 3075 cm^{-1} (Figure 4A and B). Interpretation of the EM images of cells with nanoparticles is not always self-evident. Cells can also naturally contain electron dense endogenous material that can make it difficult to distinguish nanoparticles from these endogenous structures. Also, not all nanoparticles are necessarily electron dense and therefore may not be visible in EM images. Here correlative imaging is beneficial; CARS can first be used to chemically-specifically identify nanoparticles and the correlative information from the EM images then reveals more precisely how the nanoparticles appear together with surrounding cellular structures.

The physical phenomenon of light diffraction ultimately determines the absolute resolution of conventional light microscopy and the lateral spatial resolution in ideal conditions is approximately 200–500 nm, depending on the wavelength of the light and numerical aperture (NA) of the objective.[28] However, it has been demonstrated that Raman based imaging can be used to image even smaller nanoparticles if the resulting Raman scattering signal is sufficient. This is often the case with specific materials such as gold or silicon, which enhance the signal due to the electronic properties of the materials. Four-wave mixing (FWM) microscopy is not limited to probing vibrational resonances as in the case of CARS — it is also sensitive to electronic properties of the materials. FWM electronic signal enhancement can occur when one or more of the electric fields in FWM microscopy is resonant with an electronic transition within the material. Gold and silicon nanomaterials, in particular, are effectively utilized this way. Gold nanoparticles have been imaged with FWM microscopy inside cells and it has been shown that sufficient signal for

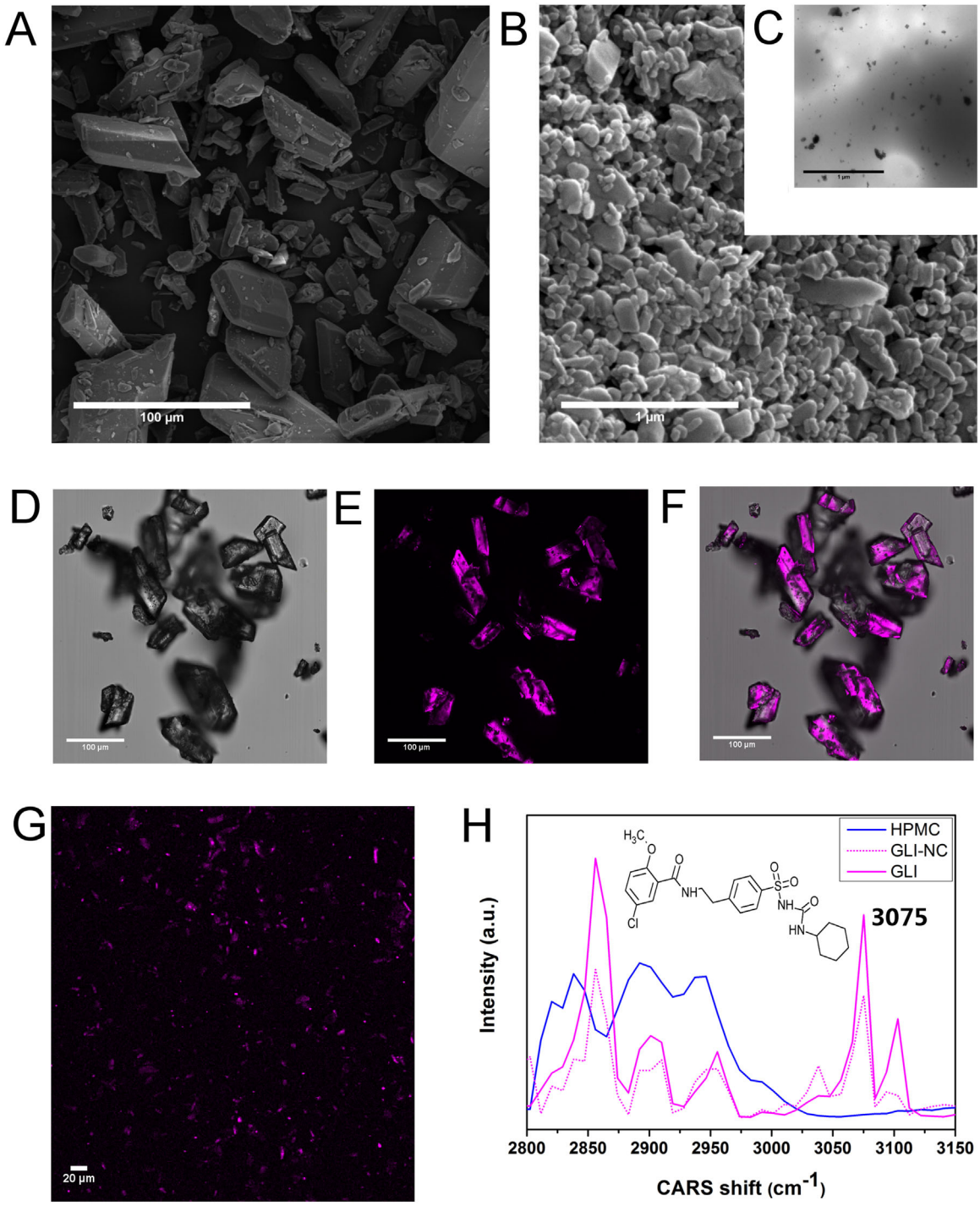

Figure 1. Material characterization. (A) SEM image of unmilled GLI crystals. (B) SEM image of dried GLI-NC suspension. (C) TEM image of dried GLI-NC suspension. (D–F) Bright field (BF) image, epi-CARS image (3075 cm^{-1}), and overlay of BF and CARS images of GLI coarse particles, respectively. (G) Epi-CARS image (3075 cm^{-1}) of GLI-NCs in aqueous medium. (H) CARS spectra of coarse GLI, GLI-NC suspension and the stabilizer, HPMC.

detection can be achieved from gold particles as small as 20 nm.[29] Plasmon-induced signal enhancement has also been used to measure the Raman signal from polymer-coated gold nanorods inside RAW 264.7 macrophages using surface-enhanced Raman scattering (SERS).[30] Nanodiamonds have also been detected inside live HeLa cells using CARS microscopy.[14] Pope et al. showed that single nanodiamonds as small as 30 nm can give a sufficient signal for detection.[14] Such strong signals are, however, ideal cases from an analytical perspective, and do not reflect the vast majority of drug nanoparticles. In the current study it was shown that individual NCs down to 500 nm give sufficient contrast in epi-CARS for

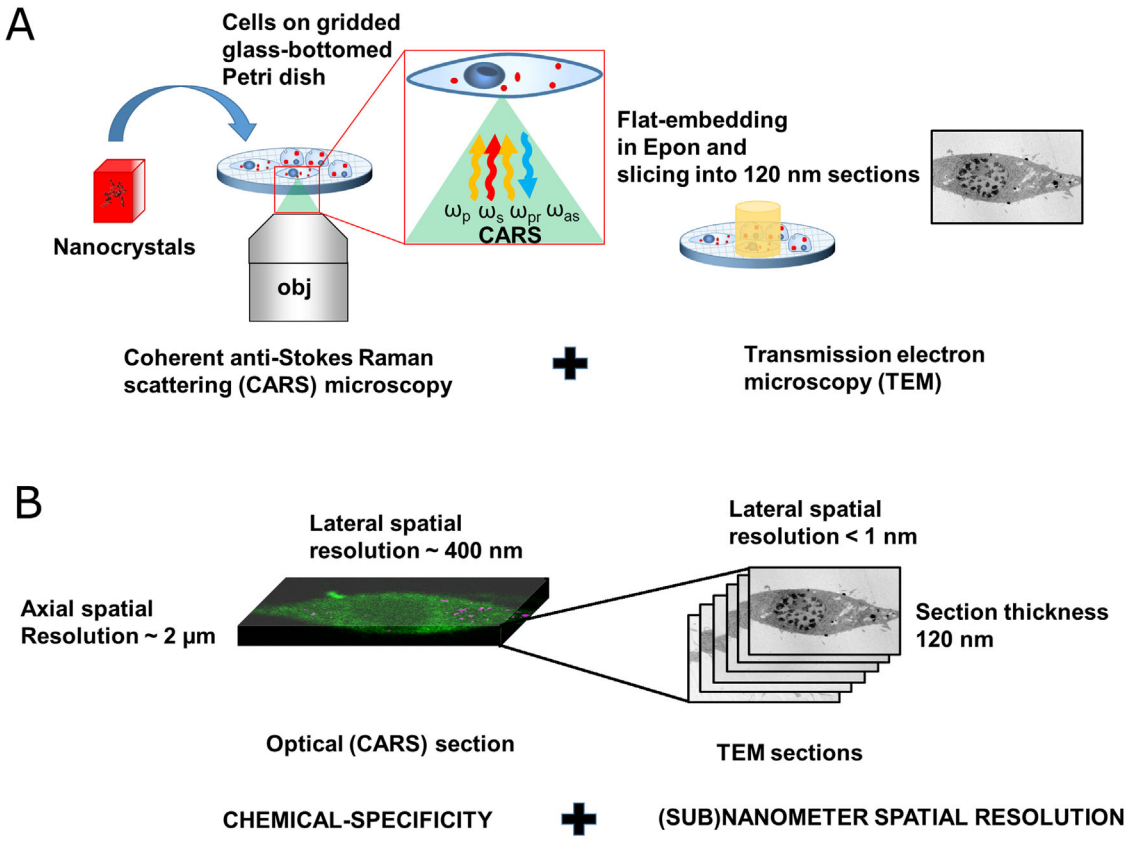

Figure 2. (A) Schematic presentation of the workflow of C-CARS-EM studies of cellular uptake of nanocrystals. Cells were cultured on gridded glass-bottomed Petri dishes allowing the same cells to be located and imaged with TEM after CARS imaging. TEM specimens were prepared while cells were still attached to the Petri dish and EM sections were prepared in the same orientation as CARS and BF imaging (flat-embedding, experimental section). (B) Schematic illustration demonstrating the resolution of optical CARS imaging and TEM.

imaging purely relying on the detection of molecular vibrations (**Figure 5**) suggesting that coherent Raman based techniques offer label-free chemically-specific imaging with suitable spatial resolution for imaging individual particles inside the cells.

The smallest details can only be seen with EM, which is the only imaging technique that can be used to truly visualize, for example, two biological membranes touching each other, as well as differentiate all the organelles in the field of view in high detail. This is beneficial because it allows, for example, the precise localization of drug nanoparticles (previously confirmed as such using CARS) to be visualized at a highly subcellular level and, therefore, access to information about the intracellular fate of nanoparticles and drug uptake mechanism(s). The information available can also be used to determine cell viability after drug treatment based on the cellular morphology changes. High magnification TEM images revealed that most of the GLI-NCs were localized in the vesicles with MVB-like morphology associated with the intraluminal vesicles (ILVs) (Figure 4C_b-E_b).[31] The (sub)-nanometer scale spatial resolution of TEM, could also be used to gain information about cell viability based on the intracellular morphology. After 6 h of incubating the cells with GLI-NCs, the cells started to show some morphological features that suggested cell damage with the fused vesicles starting to look misshapen and diluted. This cell viability information was not accessible with the conventional viability assay (Figure S5, Supporting Information), as the assay, based on the detection of luminescence signal proportional to the amount of ATP present, indicated that cell viability was up to 90% even when cells were incubated with a suspension of 1 mg mL^{-1} for 6 h.

Endocytosis can be roughly categorized as caveolae- and receptor-mediated endocytosis, micropinocytosis and phagocytosis, but other pathways are also known.[2] In general, in endocytosis, the cargo is first engulfed by primary endocytic vesicles.[31] The vesicles then undergo maturation in which they fuse to form early endosomes (EE) or early phagosomes (EP) that mature to late endosomes (LE) or late phagosomes (LP).[31] Endosomes and phagosomes can fuse together and subsequently fuse with lysosomes, then acidify and form fusions called endolysosomes or phagolysosomes, where active degradation occurs. Endolysosomes are the principal intracellular sites of acid hydrolase activity.[31,32] Endolysosomes and lysosomes are also in dynamic equilibrium in a lysosome regeneration cycle.[32] During the maturation process, the number of ILVs in endosomes increases.[31] ILVs can be found to some extent in EEs and, after a period of approximately 8–15 min, many ILVs can be found in LEs. Nanoparticles can be taken up by many of these mechanisms simultaneously.[2,33] Thus, the uptake of nanoparticles is rather complex and particle properties such as size and surface charge, as well as cell type, can all affect the uptake process.[2,34]

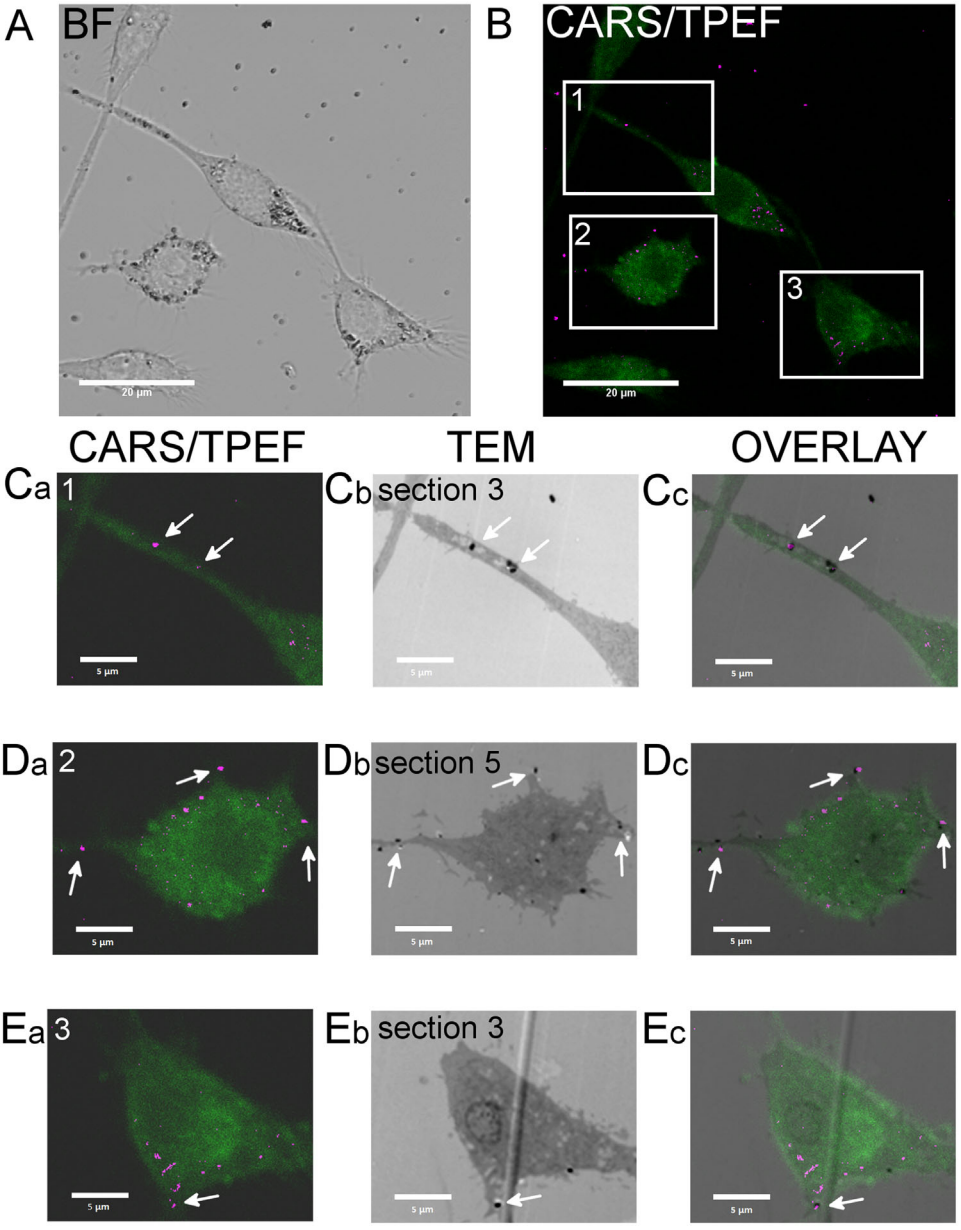

Figure 3. C-CARS-EM images of GLI-NCs in RAW 264.7 macrophages. (A) BF image and (B) corresponding CARS/TPEF image from the inside of the cell. The CARS shift at 3075 cm^{-1} was used to image GLI-NCs. TPEF originates from CellMask Orange excited with the 1064.5 nm laser. (C–E) Correlative light microscopy (CARS/TPEF) and TEM images and overlays (from left to right) from three spots shown as boxes in image B (1–3). White arrows indicate crystals that were visualized with both techniques. Scale bars are (A and B) 20 µm and (C–E) 5 µm.

In this study, it was shown that GLI-NCs were located inside vesicles with ILVs that morphologically resembled LPs and endolysosomes/phagolysosomes (Figure 4C_b-E_b).[31,32] In addition to the larger crystals visible in the CARS images, the TEM images also showed smaller dark electron-dense nano-sized (approximately 10–30 nm) particles, suggesting that the GLI-NCs may have started to dissolve or otherwise break apart in these acidic vesicles. Phagocytosis is expected to be the main internalization mechanism of particles in macrophage cells.[2]

In this study, a proof-of-principle workflow and platform was developed and proposed as an analytical platform for investigating the cellular uptake and subcellular localization of nanoparticles, as well as associated cellular changes. The feasibility of the C-CARS-EM platform for imaging nanoparticle cellular uptake was demonstrated successfully with GLI-NCs. In the C-CARS-EM procedure we have performed, whole cells were sectioned into 120 nm thick sections for TEM imaging. This allows the visualization of the entire cell, as well as all the nanocrystals taken up by the cells, with nanometer spatial resolution axially and laterally. In addition, this truly allows for correlation of the two microscopy techniques used for imaging the same cells. The lateral resolution of the CARS setup used in this study, as experimentally demonstrated by plotting the intensity profile of CARS signal of individual GLI-NC and

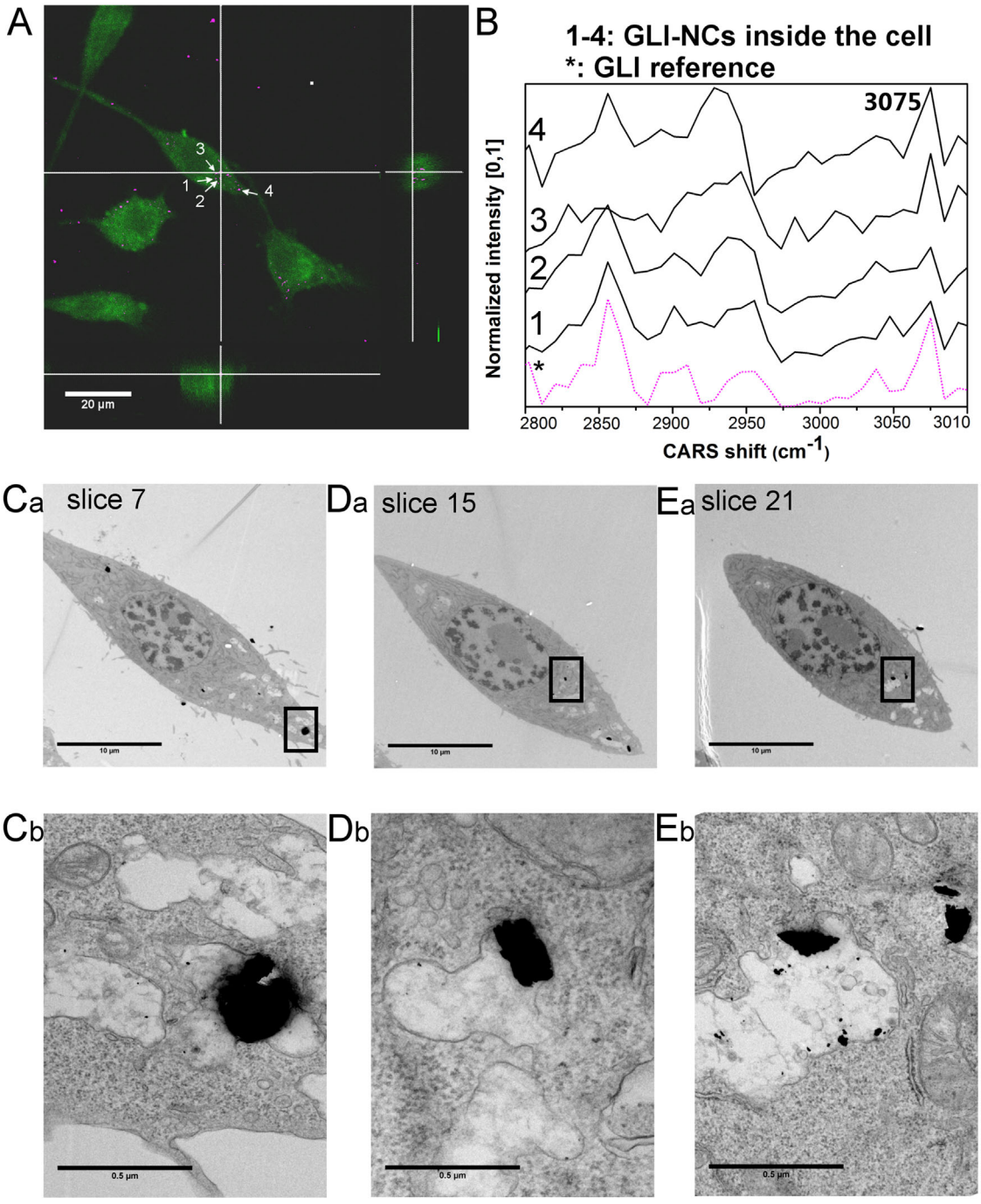

Figure 4. GLI-NC cellular uptake imaged with correlative CARS/TPEF microscopy and TEM. (A) Orthogonal projection image (CARS/TPEF) of GLI-NCs inside the RAW 264.7 macrophage. (B) CARS spectra extracted from four regions showing CARS signal at 3075 cm^{-1} from the inside of the cells as indicated by white arrows in image (A) along with a reference spectrum of GLI-NCs in aqueous medium. (C–E) Correlative TEM images of the same cell imaged with CARS/TPEF. Images Cb–Eb are higher magnification images from the regions shown as black boxes in images Ca–Ea. The position of 120 nm TEM sections are also indicated as section numbers. The total number of 120 nm TEM sections was 44. Scale bars are: (A) 20 µm, (Ca–Ea) 10 µm, and (Cb–Eb) 500 nm.

determining full width at half maximum (FWHM), was approximately 400 nm and the axial resolution was approximately 2 µm (Figure 5). This can be seen in the images of cells with nanocrystals, with the corresponding CARS/TPEF image taken from one axial plane inside the cell being compared to the TEM images obtained from 120 nm sections: the CARS images show more nanocrystals in cells compared to one TEM image. However, most of the single TEM images show nanocrystals in the cell. All the overlaid TEM slices could be visualized using a minimum projection image and video, which show a large

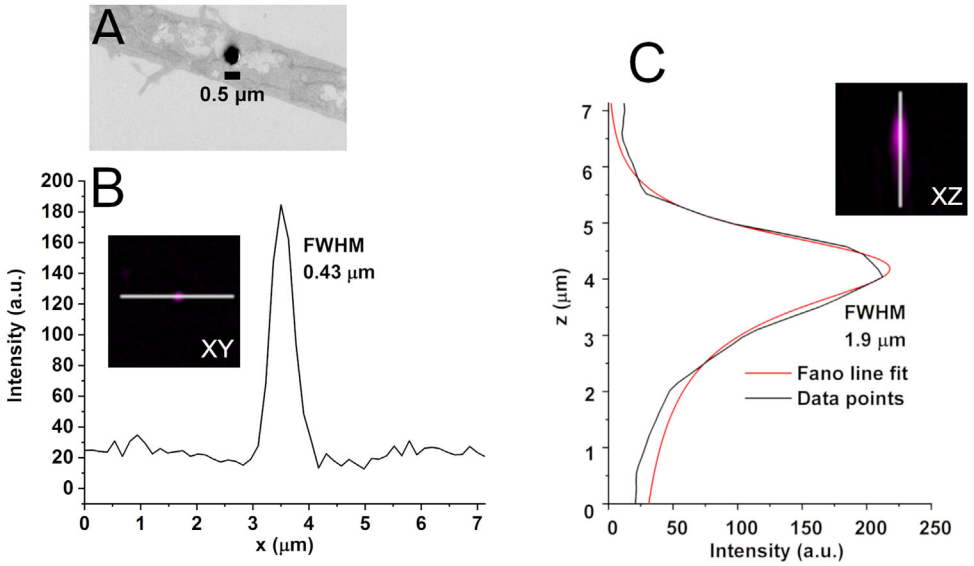

Figure 5. TEM image of an individual GLI-NC in a cell (A) and corresponding xy (B) and xz (C) CARS images (3075 cm^{-1}) of the same NC with intensity line profiles. A fanotype line fit was applied to the xz intensity data.[39] FWHM was read from the plot.

number of internalized GLI-NCs (Figure S6A and Video S1, Supporting Information). The corresponding chemically-specific maximum projection image of the CARS/TPEF z-stack from the same cell is also shown for comparison (Figure S6B, Supporting Information).

The C-CARS-EM imaging approach can be extended to other drugs and nanoparticles assuming that they generate suitable Raman signals. The proposed method could also be useful if nanoparticles lack sufficient electronic contrast, since CARS can be used to probe the nanoparticles and EM can reveal other details in cells. However, the C-CARS-EM method is the most beneficial when nanoparticles also provide electronic contrast during EM imaging. Despite the limited number of publications involving CARS analysis of cellular uptake of drug nanoparticles, the feasibility of FWM imaging has been demonstrated with some nanoparticles commonly used in drug research. These include for example silicon,[35] gold,[29] and polymeric nanoparticles[36] as well as nanodiamonds.[14] It has been shown that these materials also provide suitable electronic contrast for EM imaging. Electronic enhanced FWM microscopy has also been used to image inorganic nanocrystals[37] and CARS has been used to visualize non-fluorescent organic paliperidone palmitate nano/microcrystals in cells and tissue.[38]

In the future, it is likely that integrated microscopes capable of light microscopy and EM will become more common. Such microscopes capable of fluorescence and EM imaging already exist. [40] These systems allow faster analysis and facilitate precise colocalization of regions in the images. Potentially, CARS microscopy could also be integrated with EM.

4. Conclusions

In the present study, we developed and propose C-CARS-EM as an imaging method for studying nanoparticle drug delivery into cells by synergistically combining the benefits of two imaging methods: CARS microscopy and TEM. For the first time, a Raman-based imaging method, specifically CARS, was combined with TEM as a correlative imaging platform to image nanoparticle uptake and processing within cells. CARS offers rapid, 3D and chemically-specific imaging without labels and TEM offers (sub)-nanometer scale spatial resolution, allowing the visualization of the contents of whole cells at once and therefore also allowing the precise subcellular localization of nanoparticles. The method was used to image the uptake of GLI-NCs in RAW 264.7 macrophages. Good correlation between the CARS-active and electron-dense crystals in the CARS and TEM images was observed. The images revealed that nanocrystals were localized inside membrane bound vesicles, showing MVB-like morphology typical for LPs, endolysosomes and phagolysosomes.

The information obtained can be used to gain in depth knowledge about subtle mechanisms by which cells take up and process nanoparticles. A better understanding of these interaction processes can lead to improved and more efficient drug development, as nanoparticle fate in biological matrices can be visualized precisely in early drug development phases with cell models.

Abbreviations

API, active pharmaceutical ingredient; BF, bright field; CARS, coherent anti-Stokes Raman scattering; C-CARS-EM, correlative coherent anti-Stokes Raman scattering and electron microscopy; CLEM, correlative light-electron microscopy; DMEM, Dulbecco's Modified Eagle's Medium; EE, early endosome; EM, electron microscopy; EP, early phagosome; Epi-CARS, backwards detection of CARS signal; FWHM, full width at half maximum; FWM, four-wave mixing; HPMC, hydroxypropylmethyl cellulose; GLI, glibenclamide; GLI-NC, glibenclamide nanocrystal; LE, late endosome; LP, late phagosome; MVB, multivesicular body; SEM, scanning electron microscopy; TEM, transmission electron microscopy; TPEF, two-photon excited fluorescence.

Supporting Information

Supporting Information is available from the Wiley Online Library or from the author.

Acknowledgements

J.S. acknowledges Senior Scientist Ilya Belevich from the EM Unit for the help in processing TEM images. J.S. and C.J.S. acknowledge the University of Helsinki Research Funds for a three-year research project grant (2014–2016) and the Academy of Finland (grant no. 289398). H.A.S. acknowledges the University of Helsinki Research Funds and the European Research Council under the European Union's Seventh Framework Programme (FP/2007–2013, Grant no. 310892).

The spelling of the word (sub)-nanometer was corrected on 07 December, 2018.

Conflict of Interest

The authors declare no financial or commercial conflict of interest.

Keywords

cell imaging, cellular nanoparticle uptake, coherent anti-Stokes Raman scattering (CARS) microscopy, drug nanocrystals, non-linear imaging

Received: July 18, 2018
Revised: September 25, 2018
Published online: November 23, 2018

[1] G. Chen, I. Roy, C. Yang, P. N. Prasad, *Chem. Rev.* **2016**, *116*, 2826.
[2] H. Hillaireau, P. Couvreur, *Cell. Mol. Life Sci.* **2009**, *66*, 2873.
[3] J. W. Lichtman, J. Conchello, *Nat. Methods*. **2009**, *2*, 910.
[4] T. Tenuta, M. P. Monopoli, J. Kim, A. Salvati, K. A. Dawson, P. Sandin, I. Lynch, *PLoS ONE* **2011**, *6*, 25556.
[5] S. Kumar, R. Lahlali, X. Liu, C. Karunakaran, *Appl. Spectrosc. Rev.* **2016**, *51*, 466.
[6] a) K. C. Gordon, C. M. McGoverin, *Int. J. Pharm*. **2011**, *417*, 151; b) W. J. Tipping, M. Lee, A. Serrels, V. G. Brunton, A. N. Hulme, *Chem. Soc. Rev.* **2016**, *45*, 2075; c) H. J. Butler, L. Ashton, B. Bird, G. Cinque, K. Curtis, J. Dorney, K. Esmonde-White, N. J. Fullwood, B. Gardner, P. L. Martin-Hirsch, M. J. Walsh, M. R. McAinsh, N. Stone, F. L. Martin, *Nat. Protoc*. **2016**, *11*, 664; d) B. Kann, H. L. Offerhaus, M. Windbergs, C. Otto, *Adv. Drug Deliv. Rev.* **2015**, *89*, 71.
[7] T. Chernenko, R. R. Sawant, M. Miljkovic, L. Quintero, M. Diem, V. Torchilin, *Mol. Pharm*. **2012**, *9*, 930.
[8] a) E. Efeoglu, M. Keating, J. McIntyre, A. Casey, H. J. Byrne, *Anal. Methods* **2015**, *7*, 10000; b) J. Dorney, F. Bonnier, A. Garcia, A. Casey, G. Chambers, H. J. Byrne, *Analyst* **2012**, *137*, 1111;
[9] C. Matthäus, S. Schubert, M. Schmitt, C. Krafft, B. Dietzek, U. S. Schubert, J. Popp, *ChemPhysChem* **2013**, *14*, 155.
[10] a) J.- X. Cheng, X. S. Xie, *Science*. **2015**, *350*, aaa8870; b) C. H. Camp, Jr, M. T. Cicerone, *Nat. Photonics* **2015**, *9*, 295.
[11] J.-X. Cheng, X. S. Xie, *J. Phys. Chem. B*. **2004**, *108*, 827.
[12] A. Zumbusch, W. Langbein, P. Borri, *Prog. Lipid Res*. **2013**, *52*, 615.
[13] a) N. L. Garrett, A. Lalatsa, D. Begley, L. Mihoreanu, I. F. Uchegbu, A. G. Schätzlein, J. Moger, *J. Raman Spectrosc*. **2012**, *43*, 681; b) N. Garrett, M. Whiteman, J. Moger, *Opt. Express* **2011**, *19*, 17563.
[14] I. Pope, L. Payne, G. Zoriniants, E. Thomas, O. Williams, P. Watson, W. Langbein, P. Borri, *Nat. Nanotechnol*. **2014**, *9*, 940.
[15] a) H. D. Summers, M. R. Brown, M. D. Holton, J. A. Tonkin, N. Hondow, A. P. Brown, R. Brydson, P. Rees, *ACS Nano* **2013**, *7*, 6129; b) M. Costanzo, F. Carton, A. Marengo, G. Berlier, B. Stella, S. Arpicco, M. Malatesta, *Eur. J. Histochem*. **2016**, *60*, 107.
[16] a) A. J. Koster, J. Klumperman, *Nat. Rev. Mol. Cell Biol*. **2003**, *4 supplement*, SS6; b) E. Brown, J. Mantell, D. Carter, G. Tilly, P. Verkade, *Semin. Cell Dev. Biol*. **2009**, *20*, 910; c) R. T. Schirra, P. Zhang, *Curr. Protoc. Cytom*. **2014**, *70*, 12.36.1.
[17] a) E. Betzig, G. H. Patterson, R. Sougrat, O. W. Lindwasser, S. Olenych, J. S. Bonifacino, M. W. Davidson, J. Lippincott-Schwartz, H. F. Hess, *Science* **2006**, *313*, 1642; b) T. A. Klar, S. Jakobs, M. Dyba, A. Egner, S. W. Hell, *Proc. Natl. Acad. Sci*. **2000**, *97*, 8206.
[18] P. Liu, D. V. Chulhai, L. Jensen, *ACS Nano* **2017**, *11*, 5094.
[19] a) N. Prabhakar, M. Peurla, S. Koho, T. Deguchi, T. Näreoja, H.-C. Chang, J. M. Rosenholm, P. E. Hänninen, *Small* **2017**, *14*, 1701807; b) S. R. Hemelaar, P. De Boer, M. Chipaux, W. Zuidema, T. Hamoh, F. Perona, Martinez, A. Nagl, J. P. Hoogenboom, B. N. G. Giepmans, R. Schirhagl, *Sci. Rep*. **2017**, *7*, 1.
[20] J. Seemann, E. J. Jokitalo, G. Warren, *Mol. Biol. Cell*. **2000**, *11*, 635.
[21] I. Belevich, M. Joensuu, D. Kumar, H. Vihinen, E. Jokitalo, *PLoS Biol*. **2016**, *14*, 1.
[22] J. Blackwell, P. D. Vasko, J. L. Koenig, *J. Appl. Phys*. **1970**, *41*, 4375.
[23] H. G. M. Edwards, D. W. Farwell, A. C. Williams, *Spectrochim. Acta Part A Mol. Spectrosc*. **1994**, *50*, 807.
[24] E. Kang, J. Robinson, K. Park, J.-X. Cheng, *J. Control. Release* **2007**, *122*, 261.
[25] a) A. P. Ayala, M. W. C. Caetano, S. B. Honorato, J. Mendes, Filho, H. W. Siesler, S. N. Faudone, S. L. Cuffini, F. T. Martins, C. C. P Da Silva, J. Ellena, *J. Raman Spectrosc*. **2012**, *43*, 263; b) J. H. S. Green, *Spectrochim. Acta* **1962**, *18*, 39.
[26] J. Saarinen, E. Sözeri, S. J. Fraser-Miller, L. Peltonen, H. A. Santos, A. Isomäki, C. J. Strachan, *Int. J. Pharm*. **2017**, *523*, 270.
[27] a) A. Volkmer, J.-X. Cheng, X. S. Xie, *Phys. Rev. Lett*. **2001**, *87*, 023901; b) J.-X. Cheng, Y. K. Jia, G. Zheng, X. S. Xie, *Biophys. J*. **2002**, *83*, 502.
[28] S. W. Hell, M. Dyba, S. Jakobs, *Curr. Opin. Neurobiol*. **2004**,*14*, 599.
[29] a) F. Masia, W. Langbein, P. Watson, P. Borri, *Opt. Lett*. **2009**, *34*, 1816; b) G. Zoriniants, F. Masia, N. Giannakopoulou, W. Langbein, P. Borri, *Phys. Rev. X* **2017**, *7*, 1.
[30] D. Pissuwan, A. J. Hobro, N. Pavillon, N. I. Smith, *RSC Adv*. **2014**, *4*, 5536.
[31] a) J. Huotari, A. Heleni, *EMBO J*. **2011**, *30*, 3481; b) M. Bohdanowicz, S. Grinstein, *Physiol. Rev*. **2013**, *93*, 69.
[32] N. A. Bright, L. J. Davis, J. P. Luzio, *Curr. Biol*. **2016**, *26*, 2233.
[33] R. Firdessa, T. A. Oelschlaeger, H. Moll, *Eur. J. Cell Biol*. **2014**, *93*, 323.
[34] O. Lunov, T. Syrovets, C. Loos, J. Beil, M. Delacher, K. Tron, G. U. Nienhaus, A. Musyanovych, V. Mailänder, K. Landfester, T. Simmet, *ACS Nano* **2011**, *5*, 1657.
[35] Y. Jung, L. Tong, A. Tanaudommongkon, J.-X. Cheng, C. Yang, *Nano Lett*. **2009**, *9*, 2440.
[36] N. L. Garrett, A. Lalatsa, I. Uchegbu, A. Schätzlein, J. Moger, *J. Biophotonics* **2012**, *5*, 458.
[37] A. V. Kachynski, A. N. Kuzmin, M. Nyk, I. Roy, P. N. Prasad, *J. Phys. Chem. C. Nanomater. Interfaces* **2008**, *112*, 10721.
[38] N. Darville, J. Saarinen, A. Isomäki, L. Khriachtchev, D. Cleeren, P. Sterkens, M. van Heerden, P. Annaert, L. Peltonen, H. A. Santos, C. J. Strachan, G. Van den Mooter, *Eur. J. Pharm. Biopharm* **2015**, *96*, 338.
[39] U. Fano, *Phys. Rev*. **1961**, *124*, 1866.
[40] a) A. V. Agronskaia, J. A. Valentijn, L. F. van Driel, C. T. W. F M. Schneijdenberg, B. M. Humbel, P. M. P. van Bergen en Henegouwen, A. J. Verkleij, A. J. Koster, H. C. Gerritsen, *J. Struct. Biol*. **2008**, *164*, 183; b) F. G. A. Faas, M. Bárcena, A. V. Agronskaia, H. C. Gerritsen, K. B. Moscicka, C. A. Diebolder, L. F. van Driel, R. W. A. L. Limpens, E. Bos, R. B. G. Ravelli, R. I. Koning, A. J. Koster, *J. Struct. Biol*. **2013**, *181*, 283; c) M. A. Karreman, I. L. C. Buurmans, A. V. Agronskaia, J. W. Geus, H. C. Gerritsen, B. M. Weckhuys, *Chem – A Eur. J*. **2013**, *19*, 3846.

